# Variable Response Characteristics of a Soft Sensorized Hydrogel using Mesoscale Cellular Structures

Naoki Tano[1], Ryman Hashem[2], David Hardman[2], and Fumiya Iida[2]

*Abstract*— Sensorized hydrogels are attracting tremendous interest in the manufacture of flexible strain sensors due to their impressive responses and tunable mechanical properties. However, many require extensive fabrication processes and hazardous raw materials, making their practical application difficult. Here, we demonstrate how the parameters of mesoscale cellular mesh sensors can be varied to control and tune the response characteristics of a biocompatible gelatin-based hydrogel using a straightforward fabrication process and readily available low-cost materials. An analytical model is derived to validate the experimental results, providing a framework for the design and optimization of sensor morphologies.

Using this, 40% changes in gauge factor are demonstrated with no change in material properties, indicating that our in-plane cellular structures are a substantial and feasible method to control the sensitivity of flexible and stretchable strain sensors. We use the structures to demonstrate wearable proprioceptive devices, anisotropic bidirectional responses, and localization of a tactile stimulus.

## I. INTRODUCTION

The field of soft robotics, along with flexible strain sensors, is growing exponentially in a wide range of applications. The inherent flexibility of soft robots allows large deformations and safe interaction with humans [1], whilst the applications of soft robots are expanding including soft grippers [2], [3], bio-inspired soft robots [4], and wearable robots [5]. Consequently, any integrated strain sensors must accommodate large deformations; in the case of wearable robots, human knee joints repeatedly undergo 55 % strain while walking, which is far beyond the ∼5 % limit of conventional rigid sensors [6], necessitating the development of flexible and stretchable soft sensors.
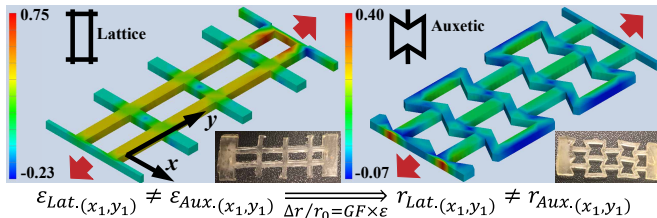


Fig. 1: Different cellular structures produce different local strain distributions. Due to this difference in strain, the measured resistance change also varies with morphology: by controlling the parameters of the unit cell, we can control the sensitivity of the hydrogel sensors.

Hydrogels - three-dimensional crosslinked polymer networks formed by natural or synthetic materials with a high water content [7] - are promising candidates for flexible strain sensor materials due to their intrinsic biocompatibility and flexibility [8], [9]. Hydrogel-based strain sensors have been exploited in the field of soft robotics research, including a wearable glove for gesture-based human-machine interfaces, and strain sensing in soft grippers or quadruped soft robots [10]. For these applications, various works have examined the tunable sensitivities of hydrogel sensors, through nanocomposites [11], [12], [13], ionic additives [14], [15], and structural optimization [16]. Gelatin-based hydrogels offer significant advantages for the fabrication of flexible sensors as they are inexpensive, biodegradable, non-hazardous, and can be engineered as multi-functional materials [17], [18], [19].

Wang et al. [20] fabricated a self-healable sensor by adding silver nanowires to a gelatin/tannic acid hydrogel, whilst Hardman et al. [21] introduced aqueous carbon black into 3D printable gelatin/glycerol hydrogel sensors. Sun et al. [22] fabricated a polyacrylamide/gelatin sensor with 2.04 GF at 600% strain, where gauge factor GF is defined: $GF = \dfrac{\Delta R/R_0}{\varepsilon}$. $\Delta R/R_0$ is the relative resistance change (RRC), and $\varepsilon$ is the strain applied to a piezoresistive sensor.

The response characteristics of soft sensor networks can be tuned via the placement of individual channels [23], [24]. However, complex morphologies arising from such optimization can be challenging to fabricate [25], [26]. Additive manufacturing is one approach to improve fabrication [27], whilst the casting of individual sensor structures provides another route to adjusting sensitivities [16], [28], [29].

In this work, we utilize a gelatin/glycerol hydrogel presented by Hardman et al. [15], which is straightforward and low-cost to fabricate, with a highly linear response to 300% strains. Furthermore, the hydrogel's 3D printability facilitates customizable mesoscale structures, enabling our investigations into their effect on the sensor response. We control the strain response characteristics by tuning the parameters of a mesoscale 2D unit cell, which is repeated within the plane to produce a macroscale sensor: Fig. 1. Unlike micro/nano-scale changes, mesoscale designs can be modified using simple fabrication processes. Still, there is minimal existing work examining the application of mesoscale design to hydrogel-based piezoresistive strain sensors.

Upon the application of a constant global strain, we design the cellular structures to produce different local strain distributions, directly affecting the sensor's strain-resistance

characteristic. Using a combination of experimental measurements and FEM simulations, we establish an analytical model consistent with our results, providing a framework for the optimization of in-plane sensor morphologies for response characteristics. Using a 100%-filled design as a baseline, we demonstrate +28%/-40% changes in the gauge factor to an applied tensile strain through simple shifts in the unit cell's morphology.

By generating these changes without shifts in the material's composition, we facilitate straightforward sensor fabrication using a consistent process: the macroscale sensors are all manufactured from the same material using one-part casting. We demonstrate the potential of this method as a design technique by introducing three applications: a proprioceptive joint sensor, an anisotropic bidirectional sensor, and a localizing skin.
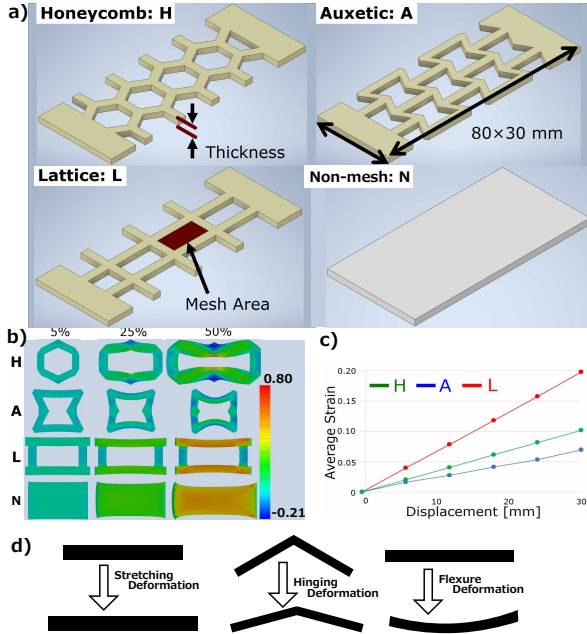
## II. SENSOR DESIGN

### A. Unit Cell Parameters



Fig. 2: a) The four tested structures: honeycomb, auxetic, lattice, and Non-mesh. b) FEM simulated strain distributions in the tensile direction of the three unit cells and non-mesh at 5, 25, & 50 % global strains. c) Average tensile strain of all elements in the FEM samples vs global displacement. d) Stretching, hinging, and flexure deformations.

As shown in Fig. 1, we test our mesoscale unit cells by measuring a sample's response to an applied tensile strain. To choose the base cells, we first categorize their deformations into three types: stretching, hinging, and flexure deformations [30] (Fig. 2-d). The stretching deformation extends the edges of the structure without angular change and is the main factor in altering the resistance change. Hinging deformation, unlike stretching deformation, changes the angles without

edge extension. As no tensile strain is generated, hinging deformation has little effect on the resistance performance. Finally, flexure deformation can be considered as a bending beam. In this deformation, one face is extended and the other compressed. Solid strain sensors without a cellular structure (henceforth referred to as 'non-mesh') have no joints and are therefore only subject to stretching deformation under tensile stress. This means that different resistance responses can be generated if the structure is subjected to hinging or flexure deformation through the appropriate design of the unit cells.

To introduce hinging deformations under applied strain, we first design a hexagonal structure ('Honeycomb in Fig. 2-a). Its design is similar to those used widely for energy absorption applications [31], [32]. By aligning the hinged edges with the principal strain axis, we expect hinging to play a part in the resistive response until the internal angles approach 180°, after which the structure would behave more similarly to Fig. 2's lattice structure, which uses rectangular unit cells to eliminate hinging deformations from the outset. Its outer horizontal bars are aligned with the internal bars, unlike the honeycomb cells in which they are offset. Finally, an auxetic unit cell is introduced to examine the combined effects of hinging and flexure deformations on the sensor characteristics. Auxetic structures are well-known in the field of metamaterials due to their negative Poisson's ratio [33] within an initial strain range: here, we examine how their piezoresistive sensor response varies with strain.

We also parameterize the design of these cell morphologies using three different cell areas and out-of-plane thickness, which is varied between 2 & 5 mm: a range that is straightforward to fabricate without interfering with sensor applications. The cell area is varied between 25, 50, and 100 $mm^2$ with a constant thickness of 2 mm, and thicker sensors are fabricated with a cell area of 100 $mm^2$.

### B. Finite Element Validation

The three unit cells described in Section II-A are validated using FEM models, built for the three structures with 100 $mm^2$ area and 2 mm thickness parameters using *Inventor Nastran* and an approximate Young's Modulus of 3 MPa [15]. Fig. 2-b shows the deformation of the closed cells under applied principal strain. Whilst the lattice cell remains rectangular, the hexagonal and auxetic cells change their angles significantly, relaxing the average element strain - which is closely associated with a physical sample's measured resistance. The auxetic cell shows an even lower average strain, undergoing both hinging and flexure deformations to relax the stresses experienced by each element. Conversely, the lattice cell extends only along its longitudinal edges with negligible hinging and flexure deformations.

To test the scaling of this effect to macroscale geometries, Fig. 2-c compares the average element strains for the three 30×60 mm structures during principally applied strains. A displacement of 6→30 mm in the longitudinal direction corresponds to 10→50% of the tensile strain of the sample.

Since the honeycomb structures facilitate hinging deformations, the element strains are smaller, with an average value of approximately 1/2 of that of the lattice structure. Similarly, the auxetic samples have the lowest average strain due to their minimal stretching during small strains.

## III. RESULTS

### A. Mesh Shape and Thickness

First, the strain responses of the four unit cells (non-mesh, honeycomb, auxetic, and lattice) with 100 mm$^2$ area and 2 mm thickness are tested. The results are shown in Fig. 3-a, where clear differences in the strain-RRC curves are visible. The gauge factor (gradient) of the lattice sample is consistently higher than the two hinging samples. These tensile test results are in good agreement with Fig. 2-c's average strain: the lattice and auxetic samples have the highest/lowest GFs, respectively. These structures are selected for subsequent testing as they show significant differences in their resistance performance compared to the baseline non-mesh sensor. This baseline fractures at 140% at the gripping position due to the high gripping force required to prevent the sensor from slipping, but behaves very similarly to the hexagonal sample before this.

Since the hexagonal samples did not show a significant difference from the non-mesh ones, the following experiments were performed using the other structures.

To demonstrate the reproducibility of these effects, Fig. 3-b plots N, A, & L during cyclic loading, validating their implementation in practical sensor applications. The small amount of hysteresis during the cyclic loading that comes from the rearrangement of conductive particles is observed in all mesh structures and the Non-mesh. More thorough analyses of the material's hysteresis behaviours have been presented in the authors' previous work [21]. Fig. 3-c plots the tensile responses of four samples showing good reproducibility throughout all shapes whilst also investigating the effect of thickness. The slight differences come from the influence of ambient conditions such as humidity and temperature.

No significant differences can be seen between the 2 & 5 mm plots, indicating that thickness is not relevant for the sample GFs, unlike the unit cell shape. Though it has no effect on the strain distribution, thickness alters the mechanical strength. This means that the strain distribution depending on the in-plane morphology is a more important determinant of sensitivity than mechanical strength, and thicknesses can be chosen to match the required strength for a given application.

### B. Mesh Area

Having seen the negligible effect of thickness on the sensor responses, we next examine the impact of mesh area: Fig. 3-d plots the GFs at 50 % strain for the A & L samples as the mesh area varies from 25 to 100 mm$^2$. The results show that as the mesh size decreases, the change in GF from the non-mesh baseline decreases for both the auxetic and the lattice structures. From this series of experiments, it was found that the lattice sample parameters had the highest GF: more than 1.28 times higher than that of the non-mesh gelatin sensors since the lattice structure can undergo only stretching deformations. Furthermore, periodic horizontal lines may contribute to enhancing the GF as they emphasize the tensile strain in longitudinal edges by relaxing strain at their nodes. On the other hand, the auxetic structure of the same group was less than 0.58 times higher than that of the non-mesh. This comes from the structure's hinging deformations.

### C. Computational Model

In Sections III-A & III-B we see how changes in the planar morphologies could be tuned to affect the sensitivities and resistive response characteristics of our sensors. A complete design pipeline would include the ability to simulate the effect of these parameters before fabrication, in order to match their effects to an application (Section III-D). Here, we propose and develop a preliminary modeling method using the experimental results from the lattice sample to validate the findings. The lattice sample is used for its easy-to-understand structure with the proposed model.

Firstly, the morphological parameters of the lattice are defined as shown in the top diagram of Fig. 4-a. The structure is then transformed into a spring model, depicted in the middle diagram of Fig. 4-a. Stiffness constants are calculated based on $k = E\dfrac{S}{l}$ where E, S, and l are Young's modulus of the material, the cross-sectional area of the edge, and the edge length, respectively. From the above equation, the stiffness constant and displacement of each edge are expressed as:

$$k_n = E\frac{b_n t}{l_n}, \quad x_n = \frac{F_n}{k_n} \tag{1}$$

where $l_n$, $b_n$, and $t$ denote the length, width, and thickness of edge n, respectively. $F_n$ is defined as the applied tensile force for edge n. Since $E$ is constant throughout the structure, the displacement ratio of each edge can be calculated based on length, width, and thickness, without Young's modulus. By taking the global strain and the strain in the $n_{th}$ edge as $\varepsilon$ and $\varepsilon_n$ respectively, the strains can be determined:

$$\varepsilon_n = \frac{\varepsilon L}{l_n} \times \frac{x_n}{\sum_i x_i}. \tag{2}$$

Additionally, the initial resistance in each section can be calculated based on Pouillet's Law: $r = \rho\dfrac{l}{S}$, where $\rho$ is the material's inherent resistivity, and $S$ and $l$ are its cross-sectional area and length. The ratio of the initial resistance can be obtained as $R_{0,n}$ since resistivity is constant throughout the sensor. The ratio of initial resistances in each edge is calculated:

$$R_{0,n} = \frac{l_n}{b_n t N} \tag{3}$$

where N is the number of parallel edges in longitudinal edges as they are the parallel resistances. When the initial global
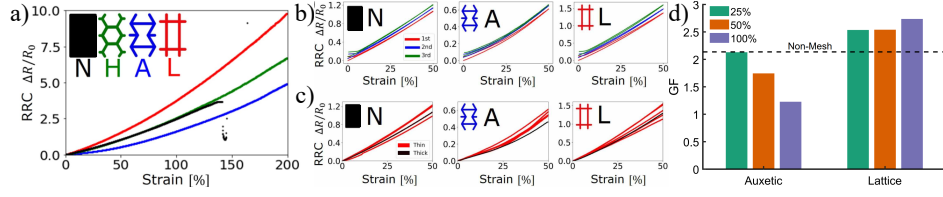
Fig. 3: a) Tensile testing of the four samples: Non-mesh (N), Honeycomb (H), Auxetic (A), and Lattice (L). b) Cyclic testing of N, A, & L samples. c) The results of reproducibility and thickness investigations. The red and black plots represent 2 & 5 mm thicknesses, respectively. d) Measured A & L GFs for mesh areas of 100, 50, and 25 mm$^2$. Y-axis is GF at 50 % strain. The black line is the GF of the non-mesh.
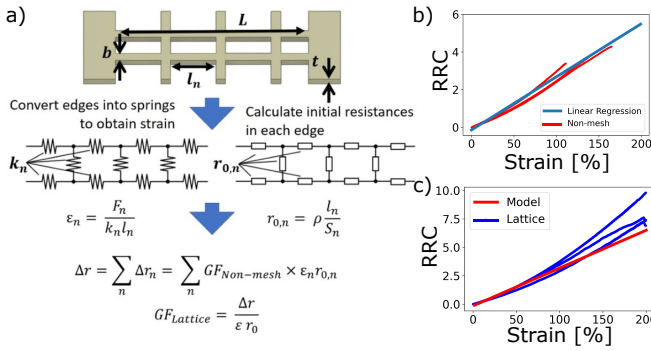


Fig. 4: a) Diagram of the computational modeling. The lattice structure is converted into a spring model to calculate strains, which are converted to resistance values. b) Linear regression for the non-mesh gelatin sensor between 10 & 120 % strains. The GF of the sample is expressed as a linear function of strain. c) A comparison of computational modeling and tensile test results.

resistance is defined as $r_0$, initial resistances in each edge can be calculated:

$$r_{0,n} = r_0 \times R_{0,n} \tag{4}$$

Now strains and initial resistances for each part are obtained, the resistance change in each edge is calculated from equations (2) & (4):

$$\Delta r_n = GF_{(\varepsilon_n)}\, r_{0,n}\, \varepsilon_n \tag{5}$$

where $GF_\varepsilon$ denotes GF of the non-mesh structure under $\varepsilon$ strain. As shown in Fig. 4-b, the RRC of the non-mesh can be expressed as $RRC_{non-mesh} = a\,\varepsilon + b$. The equation (5) can be expressed as follows:

$$\Delta r_n = (a\,\varepsilon_n + b)\, r_{0,n} \tag{6}$$

Through the above equations, it is possible to obtain overall resistance change as $\Delta r$. Then, finally, the RRC of the entire sample can be obtained through the equations (2)(4)(6) by:

$$RRC = \frac{\Delta r}{r_0} \tag{7}$$

A comparison of the lattice structure's modeled and experimental responses are shown in Fig. 4-c. The prediction

matches the measured responses for strains of up to 100%, providing a first confirmation of the effectiveness of the proposed model for the lattice structure within this range. Further developments will introduce nonlinearities into the springs to extend the predictions beyond this range, and will explicitly consider hinging and flexure deformations such that the model can be applied to all samples during the design and optimization process.

### D. Applications

To demonstrate some practical examples of mesoscale sensor design, we present three potential applications of the cellular structures developed in this work: a proprioceptive soft wearable, a bidirectional mesh sensor, and a localizing skin. Each provides a preliminary demonstration of the tunable characteristics, with the variable parameters providing adaptability to each individual use case.

One of the most common applications of flexible strain sensors is human motion detection, which can be used for a wearable device and human-machine interaction [6], [10]. Therefore, we combine the hydrogel lattice meshes and a thin silicone film for use as a proprioceptive motion detection of the elbow. Fig. 5-a shows the resulting measurements of the elbow bending angles when the composite is applied as a wearable: three progressively larger movements are clearly detectable. As the lattice structure shows increased sensitivity over the non-mesh sample (Fig. 3-a), it provides a stronger response than an equivalent non-mesh sensor, which is also plotted in Fig. 5-a.

Fig. 5-b demonstrates the bidirectional capabilities of the unit cells, which can be used to generate directional sensitivities. Strains are applied in two perpendicular directions (D1 & D2) whilst resulting GFs are measured. Clear differences are visible between the two deformation types: The lattice cell makes the difference between the two directions larger by increasing the GF of D1, whereas the auxetic gelatin sensor makes the difference smaller. This result indicates that it is possible to use two different mesh structures for different purposes. For example, an auxetic structure is preferred in case of strain from two directions needs to be detected, whilst lattice structures are suitable in maximizing the sensitivity for detecting uniaxial strains.

Moreover, the differences in sensitivities that come from varied cell structures can facilitate the localization of tactile
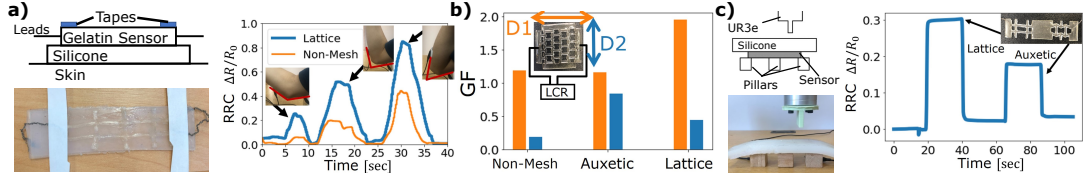
Fig. 5: a) A proprioceptive wearable device for the detection of elbow motions. b) Bidirectional GFs of three hydrogel sensors. The tensile direction of D1 is along the electrical path, whilst that of D2 is perpendicular to the path. c) A localizing skin utilizing the difference in response characteristics between the unit cells.

stimuli. To demonstrate this principle, the auxetic and lattice cells are combined to produce a localizing soft skin that detects the differences in sensitivity. Figure 5-c shows the hydrogel & silicone composite sensor, combining the two cell structures at opposite ends of the sensor. When the skin is depressed at a fixed depth by the robot arm - simulating tactile stimuli - a significant difference in response is observed between the two regions, enabling crude localization between the areas. This result demonstrates how a single mesh sensor can detect concavity at two locations, which could be used to reduce the number of sensors required across more complex skins: further work will aim to scale up this principle to a larger number of regions and bidirectional measurements, as well as exploring the effect of the silicone-hydrogel interface on the sensor's characterization.

## IV. CONCLUSIONS

In this work, we have demonstrated how mesoscale unit cells can be designed and tuned to match specific strain sensor applications, demonstrating their feasibility using an ionically sensorized gelatin hydrogel. We investigated their effect on response characteristics and presented their operation in three use applications: a proprioceptive wearable, bidirectional strain sensor, and localizing skin.

A series of tensile tests confirmed that the lattice structure had the highest GF, which was more than 1.28 times higher than that of the non-mesh gelatin sensor, whilst the auxetic structure with 100 mm$^2$ area and 2 mm thickness had a 0.58 times lower GF than the non-mesh sensor. Larger mesh areas were found to increase sensitivity change due to the large corresponding morphological change, whilst the thickness parameter was found not to affect the RRC. These results confirmed that two-dimensional morphology is one of the key factors to determine the sensitivity of the sensor due to different in-plane flexibility. A computational model was proposed and developed, matching the experimental lattice results and highlighting a promising route for future virtual unit cell design and pre-fabrication tuning. The results are expected to be applicable beyond the hydrogels tested, to a variety of flexible conductive materials such that custom sensor characteristics can be straightforwardly designed and fabricated to match a variety of applications. Further experiments will explore additional applications, hysteresis behaviours, and variation of mesoscale effects with thickness parameters via additional FEM and physical analysis.

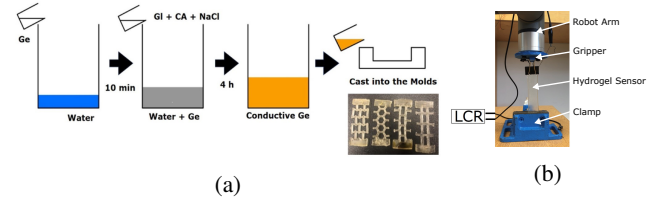## V. MATERIALS & METHODS

### A. Hydrogel Preparation



Fig. 6: Hydrogel fabrication and tensile testing.

The sensorized hydrogel was prepared by a one-pot method, as described by Hardman et al. [15]. First, 240/260 pork gelatin powder (Ge, $CakeSOS$) and cold water were mixed and allowed to bloom. 5 minutes later, glycerol (Gl, $FisherScientific$), citric acid monohydrate (CA, $FisherScientific$), and $Sainsbury's$ Table Salt (NaCl) were added whilst the temperature of the mixture was kept at 50 °C for 4 hours to form a homogeneous solution. During the homogenizing process, the beaker was covered with parafilm to prevent the evaporation of the water in the mixture. Ge, water, Gl, CA, and NaCl were mixed in the fixed proportion, which is 1:2.5:1.5:0.2:0.1 in a mass ratio, based on the previous work [15]. The mesoscale morphologies were designed using *Fusion 360* CAD software, and printed negatives were fabricated from polylactic acid (PLA) via 3D printing. To manufacture the sensors, the hydrogel was poured into the negatives at 50° and left for 24 hours to reach environmental equilibrium, after which it was peeled from the moulds.

### B. Tensile Tests

In order to assess the sensing performance of the samples throughout the experiment, tensile tests were conducted using a $Universal Robots$ UR3e as shown in Fig.6b, which applied uniaxial strain at a constant speed of 0.500 mm/s. Strain values were then calculated from the UR3e displacement data and initial length, whilst resistance values were obtained from a Keysight E4980AL Precision LCR Meter at 50k Hz with a 100 Hz sampling frequency. Cyclic tests were conducted 3 times with a maximum tensile strain of 50 % over a three-minute period. The additional resistance caused by clamping was subtracted from all measurements, and the

relative change in resistance was calculated. Matlab was used to collect the resistance data and Python 3 was used for subsequent data processing.

## VI. Acknowledgements

## VII. References

### References

[1] D. Rus and M. T. Tolley, "Design, fabrication and control of soft robots," *Nature*, vol. 521, no. 7553, pp. 467–475, 2015.

[2] Y. Tang, Y. Chi, J. Sun, T.-H. Huang, O. H. Maghsoudi, A. Spence, J. Zhao, H. Su, and J. Yin, "Leveraging elastic instabilities for amplified performance: Spine-inspired high-speed and high-force soft robots," *Science advances*, vol. 6, no. 19, p. eaaz6912, 2020.

[3] J. M. Krahn, F. Fabbro, and C. Menon, "A soft-touch gripper for grasping delicate objects," *IEEE/ASME Transactions on Mechatronics*, vol. 22, no. 3, pp. 1276–1286, 2017.

[4] C. D. Onal and D. Rus, "Autonomous undulatory serpentine locomotion utilizing body dynamics of a fluidic soft robot," *Bioinspiration & biomimetics*, vol. 8, no. 2, p. 026003, 2013.

[5] P. Polygerinos, Z. Wang, K. C. Galloway, R. J. Wood, and C. J. Walsh, "Soft robotic glove for combined assistance and at-home rehabilitation," *Robotics and Autonomous Systems*, vol. 73, pp. 135–143, 2015.

[6] T. Yamada, Y. Hayamizu, Y. Yamamoto, Y. Yomogida, A. Izadi-Najafabadi, D. N. Futaba, and K. Hata, "A stretchable carbon nanotube strain sensor for human-motion detection," *Nature nanotechnology*, vol. 6, no. 5, pp. 296–301, 2011.

[7] F. Ullah, M. B. H. Othman, F. Javed, Z. Ahmad, and H. M. Akil, "Classification, processing and application of hydrogels: A review," *Materials Science and Engineering: C*, vol. 57, pp. 414–433, 2015.

[8] X. Sun, S. Agate, K. S. Salem, L. Lucia, and L. Pal, "Hydrogel-based sensor networks: Compositions, properties, and applications—a review," *ACS Applied Bio Materials*, vol. 4, no. 1, pp. 140–162, 2020.

[9] L. Tang, S. Wu, J. Qu, L. Gong, and J. Tang, "A review of conductive hydrogel used in flexible strain sensor," *Materials*, vol. 13, no. 18, p. 3947, 2020.

[10] B. Ying, R. Z. Chen, R. Zuo, J. Li, and X. Liu, "An anti-freezing, ambient-stable and highly stretchable ionic skin with strong surface adhesion for wearable sensing and soft robotics," *Advanced Functional Materials*, vol. 31, no. 42, p. 2104665, 2021.

[11] O. Kanoun, A. Bouhamed, R. Ramalingame, J. R. Bautista-Quijano, D. Rajendran, and A. Al-Hamry, "Review on conductive polymer/cnts nanocomposites based flexible and stretchable strain and pressure sensors," *Sensors*, vol. 21, no. 2, p. 341, 2021.

[12] Z. Deng, T. Hu, Q. Lei, J. He, P. X. Ma, and B. Guo, "Stimuli-responsive conductive nanocomposite hydrogels with high stretchability, self-healing, adhesiveness, and 3d printability for human motion sensing," *ACS applied materials & interfaces*, vol. 11, no. 7, pp. 6796–6808, 2019.

[13] X. Sun, F. Yao, and J. Li, "Nanocomposite hydrogel-based strain and pressure sensors: a review," *Journal of Materials Chemistry A*, vol. 8, no. 36, pp. 18605–18623, 2020.

[14] K. Tian, J. Bae, S. E. Bakarich, C. Yang, R. D. Gately, G. M. Spinks, M. in het Panhuis, Z. Suo, and J. J. Vlassak, "3d printing of transparent and conductive heterogeneous hydrogel–elastomer systems," *Advanced Materials*, vol. 29, no. 10, p. 1604827, 2017.

[15] D. Hardman, T. George Thuruthel, and F. Iida, "Self-healing ionic gelatin/glycerol hydrogels for strain sensing applications," *NPG Asia Materials*, vol. 14, no. 1, pp. 1–13, 2022.

[16] X. Huang, Z. Yin, and H. Wu, "Structural engineering for high-performance flexible and stretchable strain sensors," *Advanced Intelligent Systems*, vol. 3, no. 5, p. 2000194, 2021.

[17] J. Shintake, H. Sonar, E. Piskarev, J. Paik, and D. Floreano, "Soft pneumatic gelatin actuator for edible robotics," in *2017 IEEE/RSJ International Conference on Intelligent Robots and Systems (IROS)*, pp. 6221–6226, IEEE, 2017.

[18] M. Baumgartner, F. Hartmann, M. Drack, D. Preninger, D. Wirthl, R. Gerstmayr, L. Lehner, G. Mao, R. Pruckner, S. Demchyshyn, *et al.*, "Resilient yet entirely degradable gelatin-based biogels for soft robots and electronics," *Nature Materials*, vol. 19, no. 10, pp. 1102–1109, 2020.

[19] X. Fan, J. Geng, Y. Wang, and H. Gu, "Pva/gelatin/$\beta$-cd-based rapid self-healing supramolecular dual-network conductive hydrogel as bidirectional strain sensor," *Polymer*, vol. 246, p. 124769, 2022.

[20] J. Wang, F. Tang, Y. Wang, Q. Lu, S. Liu, and L. Li, "Self-healing and highly stretchable gelatin hydrogel for self-powered strain sensor," *ACS applied materials & interfaces*, vol. 12, no. 1, pp. 1558–1566, 2019.

[21] D. Hardman, J. Hughes, T. G. Thuruthel, K. Gilday, and F. Iida, "3d printable sensorized soft gelatin hydrogel for multi-material soft structures," *IEEE Robotics and Automation Letters*, vol. 6, no. 3, pp. 5269–5275, 2021.

[22] X. Sun, F. Yao, C. Wang, Z. Qin, H. Zhang, Q. Yu, H. Zhang, X. Dong, Y. Wei, and J. Li, "Ionically conductive hydrogel with fast self-recovery and low residual strain as strain and pressure sensors," *Macromolecular Rapid Communications*, vol. 41, no. 13, p. 2000185, 2020.

[23] A. Krause, A. Singh, and C. Guestrin, "Near-optimal sensor placements in gaussian processes: Theory, efficient algorithms and empirical studies," *Journal of Machine Learning Research*, vol. 9, no. Feb, pp. 235–284, 2008.

[24] S. G. Nurzaman, U. Culha, L. Brodbeck, L. Wang, and F. Iida, "Active sensing system with in situ adjustable sensor morphology," *PLoS One*, vol. 8, no. 12, p. e84090, 2013.

[25] T. G. Thuruthel, J. Hughes, and F. Iida, "Joint entropy-based morphology optimization of soft strain sensor networks for functional robustness," *IEEE Sensors Journal*, vol. 20, no. 18, pp. 10801–10810, 2020.

[26] D. Hardman, T. George Thuruthel, A. Georgopoulou, F. Clemens, and F. Iida, "3d printable soft sensory fiber networks for robust and complex tactile sensing," *Micromachines*, vol. 13, no. 9, 2022.

[27] A. Georgopoulou and F. Clemens, "Pellet-based fused deposition modeling for the development of soft compliant robotic grippers with integrated sensing elements," *Flexible and Printed Electronics*, vol. 7, p. 025010, 6 2022.

[28] Y. Li, S. Luo, M.-C. Yang, R. Liang, and C. Zeng, "Poisson ratio and piezoresistive sensing: a new route to high-performance 3d flexible and stretchable sensors of multimodal sensing capability," *Advanced Functional Materials*, vol. 26, no. 17, pp. 2900–2908, 2016.

[29] J. Shintake, T. Nagai, and K. Ogishima, "Sensitivity improvement of highly stretchable capacitive strain sensors by hierarchical auxetic structures," *Frontiers in Robotics and AI*, vol. 6, 2019.

[30] D. Attard and J. N. Grima, "Modelling of hexagonal honeycombs exhibiting zero poisson's ratio," *physica status solidi (b)*, vol. 248, no. 1, pp. 52–59, 2011.

[31] G. Sun, H. Jiang, J. Fang, G. Li, and Q. Li, "Crashworthiness of vertex based hierarchical honeycombs in out-of-plane impact," *Materials & Design*, vol. 110, pp. 705–719, 2016.

[32] S. Hou, Q. Li, S. Long, X. Yang, and W. Li, "Design optimization of regular hexagonal thin-walled columns with crashworthiness criteria," *Finite elements in analysis and design*, vol. 43, no. 6-7, pp. 555–565, 2007.

[33] X. Ren, R. Das, P. Tran, T. D. Ngo, and Y. M. Xie, "Auxetic meta-materials and structures: a review," *Smart materials and structures*, vol. 27, no. 2, p. 023001, 2018.